Impact of the influenza protein PB1-F2 on the biochemical composition of human epithelial cells revealed by synchrotron Fourier transform infrared spectromicroscopy

Olivier Leymarie, Ronan Le Goffic, Frederic Jamme, Christophe Chevalier

Peer Reviewed Paper openaccess Special Issue on Spectral Imaging in Synchrotron Light Facilities

Impact of the influenza protein PB1-F2 on the biochemical composition of human epithelial cells revealed by synchrotron Fourier transform infrared spectromicroscopy

Olivier Leymarie,[a]* Ronan Le Goffic,[b] Frédéric Jamme[c] and Christophe Chevalier[d]*

[a]VIM, INRA, Université Paris-Saclay, 78350, Jouy-en-Josas, France. E-mail: olivier.leymarie@inra.fr, https://orcid.org/0000-0001-8670-3089

[b]VIM, INRA, Université Paris-Saclay, 78350, Jouy-en-Josas, France. https://orcid.org/0000-0002-2012-0064

[c]Synchrotron SOLEIL, L'Orme des Merisiers, 91190 Saint-Aubin, Gif-sur Yvette, France. https://orcid.org/0000-0002-7398-7868

[d]VIM, INRA, Université Paris-Saclay, 78350, Jouy-en-Josas, France. E-mail: christophe.chevalier@inra.fr, https://orcid.org/0000-0003-3231-9027

PB1-F2 is a non-structural protein of influenza A viruses (IAV) that modulates viral pathogenesis in a host-specific manner. In mammals, this protein has been shown to increase IAV virulence by delaying the early immune response and, eventually, exacerbating lung inflammation at the late stage of infection. PB1-F2 is a small protein, but displays very high sequence polymorphism and sequence length disparity depending on viral strain. These features result in strong variations in the cellular activity of PB1-F2. Studies have also reported that the effect of PB1-F2 is cell-type dependent. It has notably been shown that PB1-F2 can promote apoptosis in immune cells, but not in epithelial cells. This phenomenon appears to be partly related to the higher order structure of the protein, given that the presence of PB1-F2 β-aggregated structures in infected immune cells correlates with cell death induction. In this work, we evaluated, by synchrotron Fourier transform infrared spectromicroscopy, the impact of the transient expression of PB1-F2 on the biochemical composition of the human epithelial cell line HEK293T. Two PB1-F2 variants that are closely related to each other but derived from a strain with high [A/BrevigMission/1/1918 (H1N1)] or a low [A/WSN/1933 (H1N1)] virulence were studied here. Infrared spectra analysis revealed no specific enrichment of β-aggregated structures in PB1-F2-expressing cells. Nevertheless, this analysis suggested that there is a higher content of β-sheet secondary structures in the PB1-F2 from A/WSN/1933 than that from A/BrevigMission/1/1918. Our data also showed no change in membrane composition in the presence of PB1-F2, implying that PB1-F2 does not promote apoptosis in HEK293T cells. Finally, we found that the PB1-F2 from A/WSN/1933 interferes with adenosine triphosphate production, suggesting that this PB1-F2 variant may disturb the mitochondrial activity.

Keywords: influenza virus, PB1-F2, Fourier transform infrared (FT-IR), amyloid, oligomerisation, spectromicroscopy, synchrotron radiation experiment

Correspondence
Olivier Leymarie (olivier.leymarie@inra.fr) and Christophe Chevalier (christophe.chevalier@inra.fr)

Received: 22 May 2019
Revised: 10 October 2019
Accepted: 12 October 2019
Publication: 18 October 2019
doi: 10.1255/jsi.2019.a18
ISSN: 2040-4565

Citation
O. Leymarie, R. Le Goffic, F. Jamme and C. Chevalier, "Impact of the influenza protein PB1-F2 on the biochemical composition of human epithelial cells revealed by synchrotron Fourier transform infrared spectromicroscopy", *J. Spectral Imaging* **8,** a18 (2019). https://doi.org/10.1255/jsi.2019.a18

Introduction

Every year, 2–10% of the human population is affected by seasonal flu.[1] Three to five million patients suffer from severe respiratory illness that necessitates hospitalisation and causes the death of 300,000–500,000 persons.[1] Influenza A viruses (IAV), along with influenza B viruses, are the etiological agents of these epidemics. IAV are members of the Orthomyxovirus family that share the common characteristics of being enveloped viruses containing a segmented negative-sense ribonucleic acid (RNA) genome. IAV display a wide diversity of viral strains and are divided into subtypes on the basis of molecular differences of the two viral surface glycoproteins, hemagglutinin (HA) and neuraminidase (NA). So far, 18 HAs and 11 NAs have been determined, with the possibility of a hundred combinations (e.g., H1N1, H7N9, H18N11 etc.). IAV have a broad host range since they can infect humans, terrestrial and aquatic mammals, as well as avian species.[2] Each IAV strain is usually well adapted to a specific species or a small group of host species but can occasionally cross the species barrier.[2] This phenomenon can pose a serious threat to public health when the human population lacks a pre-existing or a cross-protective immunity against a species-crossing virus.[3] In this case, the virus circumvents the herd immunity developed against human strains and spreads efficiently from person to person. Such an outbreak can lead to a pandemic scenario if not contained rapidly, generally resulting in abnormally high mortality rates. Since the beginning of the 20th century, four flu pandemics have occurred: in 1918, 1957, 1968 and 2009. The "Spanish flu" pandemic of 1918 was the most devastating of these pandemics, infecting a third of the human population and causing the death of 40–100 million people worldwide.[4]

Several molecular hallmarks associated with the mammalian adaptation of IAV have been identified.[2,5] It has notably been shown that the length of the small viral protein PB1-F2 (polymerase basic 1-frame 2) is reduced in human strains when compared to avian strains.[6] Analysis of more than 7500 PB1-F2 sequences highlighted that 8.6% and 38.8% of avian and human strains, respectively, encode a non-functional protein (≤79 amino acids).[6] The same phenomenon also occurs in pig, among which 52.7% of isolated strains encode a truncated PB1-F2.[6] In addition, the presence of a full-length PB1-F2 sequence in swine IAV does not lead necessarily to PB1-F2 expression, due to a translational regulation mechanism involving sequences present downstream of the PB1-F2 initiation codon.[7] Investigations conducted by our group and others suggest that expression of a functional PB1-F2 during infection leads to an exacerbated, and deleterious, inflammatory response in a mammalian host.[8–15] Conversely, expression of a functional PB1-F2 reduces inflammatory response in the infected avian host, favouring survival of animals and viral spreading.[16–18] These observations reveal the dual role of PB1-F2 in viral fitness depending on the host type. PB1-F2 is advantageous for IAV propagation in avian hosts but deleterious in mammalian hosts. This feature explains, in part, the loss of a functional PB1-F2 in mammalian strains.

Several residues on PB1-F2 have been ascribed to a proinflammatory signature in mammals. It has notably been shown that some highly pathogenic IAV (HPAIV), such as the 1918 pandemic virus, have an asparagine-to-serine substitution at position 66 of PB1-F2 that contributes to an exacerbated inflammatory response at the late stage of the infection.[19,20] The 1918 virus, as well as the 1957 and 1968 pandemic strains, also possesses four specific amino acids (leucine, arginine, arginine and leucine at position 62, 75, 79 and 82, respectively) that are associated with an inflammatory signature but are no longer present in circulating human IAV.[21] Reintroduction of these residues in the PB1-F2 sequence from a more recent human IAV increases mortality of infected mice.[22] Furthermore, the intranasal inoculation of mice with this mutated PB1-F2 peptide induces an abnormally high production of proinflammatory cytokines and a deleterious recruitment of neutrophils in the lung, compared to wild-type PB1-F2 peptide.[22] The exacerbated inflammatory response triggered by PB1-F2 has been shown to be partly related to the activation of the nucleotide-binding domain and leucine-rich repeat containing (NLR) family pyrin domain containing 3 (NLRP3) inflammasome pathway.[12,14] The NLRP3 inflammasome is a multifactor complex responsible for activating the caspase-1 protein which induces maturation and secretion of interleukine (IL)-1β and IL-18. These two inflammatory cytokines promote recruitment of neutrophils, macrophages and monocytes to the site of infection. Formation of the NLRP3 inflammasome can be stimulated by various signals such as pathogen-associated molecular patterns (PAMPs), extracellular adenosine triphosphate (ATP), pore-forming toxin, mitochondrial damages or protein aggregates.[23–25] In that regard, data presented by

McAuley *et al.* highlight that only PB1-F2 aggregates activate the NLRP3 inflammasome.[12]

Interestingly, previous work from our laboratory has revealed that PB1-F2 adopts a variety of conformations depending on the physico–chemical conditions of the environment.[26–28] Thus, while in aqueous solution (i.e. acidic condition), PB1-F2 displays a disordered conformation, in membrane-mimetic environments [such as sodium dodecyl sulfate (SDS) or asolectin liposomes], PB1-F2 is enriched in β-sheet structures. PB1-F2 then contains 22–80 % of β-sheet structures depending on the amino acid sequence of PB1-F2.[26] Remarkably, in the presence of SDS, asolectin liposomes or negatively charged lipid membranes, β-sheet-enriched PB1-F2 oligomerises into amyloid-like fibres (i.e. β-sheet protein aggregates). These fibres have a length ranging from 100 nm to 1 µm. Of note, the C-terminal domain of PB1-F2 (amino acids 53 to 90), which is intrinsically disordered in acidic condition, spontaneously undergoes a structural reorganisation toward amyloid-like structures in neutral and basic condition.[29] In contrast, the full-length PB1-F2 or the N-terminal domain of the protein (amino acids 1 to 52) form amorphous aggregates in these conditions. This work has also revealed that the C-terminal domain of PB1-F2, but not the N-terminal domain of PB1-F2 or the pre-polymerised-PB1-F2 amyloid fibres, can permeabilise cellular membranes, reducing cell viability. Interestingly, a cytotoxic effect is observed on cells treated with sonication-fragmented PB1-F2 amyloid fibres as well. This effect is similar to that seen with the PB1-F2 C-terminal domain, suggesting that the amyloid fibre fragments are responsible for the PB1-F2-induced cytotoxicity.

In a previous work, we have identified the presence of PB1-F2 amyloid fibres within IAV-infected human monocytes by using synchrotron Fourier transform infrared (sFT-IR) spectromicroscopy.[30] The switch of PB1-F2 from a monomeric state to amyloid fibres appears to be partial at the early stage of the infection [8 h post-infection (pi)] but complete at 24 h pi, leading to an accumulation of aggregated structures. sFT-IR spectromicroscopy also revealed perturbations of cellular membrane and a loss of membrane fluidity that are associated with PB1-F2 expression in a cell-dependent manner. FT-IR microscopy is a very powerful tool to analyse subtle biochemical changes in cells.[31–33] The technique relies on the fact that when infrared light goes through organic or inorganic materials, it induces the vibrational excitation of molecules, resulting in specific absorption bands in the IR spectrum. Proteins, lipids or nucleic acids have thus distinguishing IR spectrum signatures, allowing slight modifications of each of these compounds in biological samples to be evaluated.[34] FT-IR spectroscopy is particularly sensitive for the determination of the structural conformation of proteins (e.g. α-helix, β-sheets, β-turns etc.). FT-IR spectromicroscopy offers the advantage of performing FT-IR spectroscopy on single cells or specific areas of a sliced tissue preparation. This technique has notably been shown to be efficient for the detection of cells infected with various types of viruses.[35–38] Usually, FT-IR spectromicroscopy is limited in term of spatial resolution because of the brightness of the thermal infrared source.[39] However, a synchrotron IR source has a very high brightness (100–1000 times higher than a conventional one), allowing us to work near diffraction-limited spatial resolution with an excellent signal-to-noise ratio.[34]

Although, the contribution of PB1-F2 in the immunopathology of IAV infection is well documented, little is known about the molecular activity of PB1-F2 and its structural behaviour. In the present study, we evaluate by sFT-IR spectromicroscopy the conformation of PB1-F2 and the impact of this protein on the cellular integrity of human epithelial cells in the absence of viral context. Using two closely related PB1-F2 variants from pandemic and seasonal IAV, we show that i) PB1-F2 by itself does not form β-amyloid fibres nor disturb cellular membrane composition in epithelial cells, contrary to what has been described in immune cells; and ii) PB1-F2 alters ATP production in mitochondria in a strain-dependent manner.

Materials and methods

Cell line

HEK293T cells were propagated and sub-cultured in Dulbecco's modified Eagle's medium (Gibco) supplemented with 10 % decomplemented foetal calf serum, 2 mM L-glutamine 1 %, 100 µg mL^{-1} streptomycin and 100 UI mL^{-1} penicillin. Cell culture was maintained at 37 °C in 5 % CO_2 incubator.

Plasmid constructions

The PB1-F2 constructions were obtained by cloning the coding sequence of the PB1-F2 A/WSN/1933 (H1N1)

and PB1-F2 A/BrevigMission/1/1918 (H1N1) strains in doxycycline-inducible pTRE-tight vector (Takara Bio, USA). Gene-specific 5′ and 3′ primers containing the EcoRI and BamHI restriction site, respectively, were used to amplify the open reading frame of each gene. The gene encoding PB1-F2 A/WSN/1933 (H1N1) was provided by Dr Ervin Fodor (University of Oxford, Oxford, UK). The PB1-F2 A/BrevigMission/1/1918 (H1N1) coding sequence was artificially synthesised. All PB1-F2 constructions were verified by automated sequencing performed by MWG (Ebersberg, Germany).

Cell transfections

HEK293T were grown on zinc-selenide 4-mm diameter IR transparent windows at 37 °C in 5 % CO_2 incubator. The cells were transiently co-transfected with the pTET-ON plasmid (Takara Bio, USA) and doxycycline-inducible plasmids expressing, or not (empty pTRE-tight vector), PB1-F2 variants of the A/WSN/1933 (H1N1) and A/BrevigMission/1/1918 (H1N1) strains. Transfections were performed using the Fugene HD transfection reagent (Roche) following the manufacturer's instructions. Twenty-four hours post-transfection, the cells were treated with 1 µg mL^{-1} doxycycline (BD Bioscience) for 24 h at 37 °C, and then fixed with 4 % paraformaldehyde in phosphate buffered saline for 20 min.

Synchrotron FT-IR spectromicroscopy

Synchrotron FT-IR spectromicroscopy was performed at the SOLEIL Synchrotron (Gif-sur-Yvette, France) using the SMIS beamline (Synchrotron SOLEIL) as previously described.[30] All spectra were recorded in transmission mode on a Nicolet Continuum XL microscope (Thermo Scientific). The microscope comprises a motorised sample stage and a liquid nitrogen-cooled mercury cadmium telluride (MCT-A) detector (50 µm element size). The microscope operates in confocal mode using a 32× infinity corrected Schwarzschild objective (NA = 0.65) and a matching 32× condenser. All IR spectra were recorded using a dual mask aperture of 10 × 10 µm^2. Individual spectra were saved in log (1/*R*) format at 4 cm^{-1} spectral resolution, with 128 co-added scans encompassing the mid-IR region from 4000 cm^{-1} to 800 cm^{-1}. Seventy-five single-cell spectra were recorded for each experimental condition. All IR spectra were processed with the OMNIC (Thermo Fisher Scientific) and Unscrambler (CAMO Process AS) software. Spectra presenting a large baseline deformation were removed, leading to the elimination of 14, 13 and 15 spectra for the control, PB1-F2 1918 and PB1-F2 WSN conditions, respectively. IR spectra were converted into second derivative spectra by using the Savitzky–Golay method (nine smoothing points) to enhance the spectral resolution of the absorption bands. Delimited regions of the spectrum in second derivative IR spectra were unit vector normalised and analysed by principal component analysis (PCA). The computation of principal components was based on the non-linear iterative partial least squares (NIPALS) algorithm and the model was validated with the leverage correction method.[40] Loading plots generated by the PCA analysis allowed us to identify peak positions of the absorption bands that accounted for the variations observed between experimental conditions.

Results and discussion

Experimental set-up

To determine to what extent PB1-F2 expression interferes with cell viability regardless of the contribution of the other IAV proteins, a human epithelial cell line derived from embryonic kidney (HEK293T) was transfected with doxycycline-inducible expression vectors encoding, or not, PB1-F2 variants and biochemical changes were studied by sFT-IR spectromicroscopy at the single-cell level. The analysis was performed on fixed HEK293T cells, after inducting expression of PB1-F2 by addition of doxycycline for 24 h. HEK293T cells are not the natural targets for IAV infection but provide the advantage of being easily transfectable, allowing us to reach a transfection efficiency close to 90–100 %. This parameter is essential for the relevance of the sFT-IR spectromicroscopy analysis since we decided not to perform any staining of PB1-F2 in HEK293T cells to preserve as much as possible the native state of the cells. Two PB1-F2 variants derived from A/WSN/1933 (H1N1) (WSN) and A/Brevig Mission/1/1918 (H1N1) (1918) strains were included in the present work. The WSN strain is a well-studied laboratory virus resulting from the adaptation to the mouse of the first human seasonal IAV isolate,[41] while the 1918 strain is the causative agent of the "Spanish flu" influenza pandemic.[42] Phylogenetic analyses of H1N1 subtype viruses have shown that these two strains are very closely related,[42,43] However, studies have suggested that PB1-F2 1918 may have been a major contributor to the abnormally high mortality rate

observed during the pandemic.[19,44,45] Consequently, we thought it might be interesting to compare PB1-F2 variants from the 1918 pandemic virus and a closely related seasonal virus. The amino acid sequences of PB1-F2 WSN and PB1-F2 1918 have a high percentage of identity (89 %) as shown in Figure 1. However, a marked difference is observed between the C-terminal domains of the two proteins in a region that has been identified as essential for the proinflammatory activity of PB1-F2,[21] its mitochondrial localisation[46–49] and its ability to form channel pores in lipid membranes.[50] Thus, we note the presence in the sequence of PB1-F2 1918 of five out of the five residues previously associated with an enhanced inflammation (L62, R75, R79, L82 and S66),[21] while only three of them (R75, R79 and L82) are present in PB1-F2 WSN. Conversely, PB1-F2 WSN, but not PB1-F2 1918, possesses the I68-L69-V70 motif which has been described as increasing PB1-F2-mediated cell cytotoxicity, inducing the mitochondrial localisation of the protein and extending its protein half-life.[49,51–53]

To evaluate the impact of the transient expression of PB1-F2 on cell viability, 75 IR spectra in the 4000–800 cm^{-1} region were collected for each condition studied (empty-vector, PB1-F2 1918 and PB1-F2 WSN) with a Nicolet Continuum XL microscope using a synchrotron radiation IR light source. Since HEK293T cells do not form homogenous cell layers (Figure 2A), we paid attention to select cells presenting morphological similarities not to introduce a bias in our analysis. Infrared spectra were filtered (Figure 2B) to eliminate those exhibiting a large sinusoidal oscillation in their baseline due to the Mie-type scattering, a phenomenon that can alter the intensity and position of absorption bands.[54] A Savitzky–Golay second derivative was then performed on spectra to reveal minor absorption peaks that are not resolved in raw spectra (Figure 2C). Given that a large set of values was generated by the sFT-IR spectromicroscopic measurements, the data were processed by PCA to identify the variables (i.e. wavenumbers here) that contribute to the segregation of the three experimental conditions. To do this, PCA defines new variables, called "principal components" (PCs), to explain the variance observed between samples in a dataset.[55] Each PC delineates a dimension (i.e. an axis) that explains a part of the variability. PCs form a succession of uncorrelated axes (i.e., orthogonal to each other) in the descending order of the explained variance. The first PC (PC1) accounts for the majority of the variability in a dataset and each consecutive PC accounts for the highest remaining variability. Consequently, each sample (i.e. single-cell spectrum here) can be positioned in a multidimensional space formed by PC-axes. A 2D-representation of these subspaces, called a "score plot", enables us to easily visualise the distribution of samples. In addition, each PC is associated to "a loading plot" that indicates which variables contribute the most to the determination of that PC.

PB1-F2 does not induce the formation of aggregated β-sheet structures in HEK293T cells

In our previous work,[30] sFT-IR spectromicroscopy has revealed the presence of aggregated β-sheet structures in a human monocytic cell line (U937) infected with WSN virus only when the virus was able to express PB1-F2 (wild-type WSN virus). This feature appeared to be cell-type specific since such structures were not detected when two human epithelial cell lines (A549 and HeLa cells) were infected with wild-type WSN virus.[30] To evaluate changes in the secondary structure of proteins in PB1-F2-transfected HEK293T cells, IR spectra were submitted to PCA analysis in the amide I (ranging from 1700 cm^{-1} to 1600 cm^{-1}) and amide II (ranging from 1570 cm^{-1} to 1480 cm^{-1}) regions of the spectrum. These regions are particularly sensitised to the C=O (amide I) and C–N (amide II) stretching of the protein backbone.[56] Unfortunately, PCA performed in the amide I region failed to segregate the PB1-F2 WSN, PB1-F2 1918 and control clusters (Figure S1). PCA analysis in the amide II

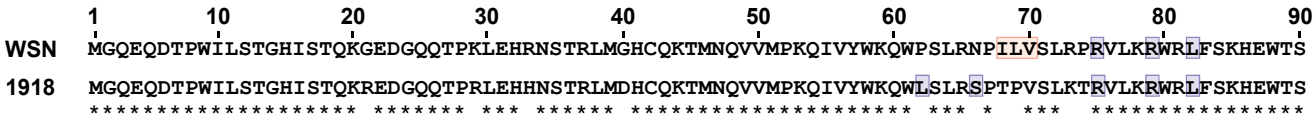

Figure 1. Amino acid sequence alignment of PB1-F2 from A/WSN/1933 (H1N1) (WSN) and A/Brevig Mission/1/1918 (H1N1) (1918) viruses. Identical amino acid residues are indicated by an asterisk. The amino acid residues associated with a proinflammatory signature of PB1-F2 are highlighted in blue. The amino acid motif associated with an increased cytotoxicity of PB1-F2 and a mitochondrial localisation of the protein are highlighted in orange.

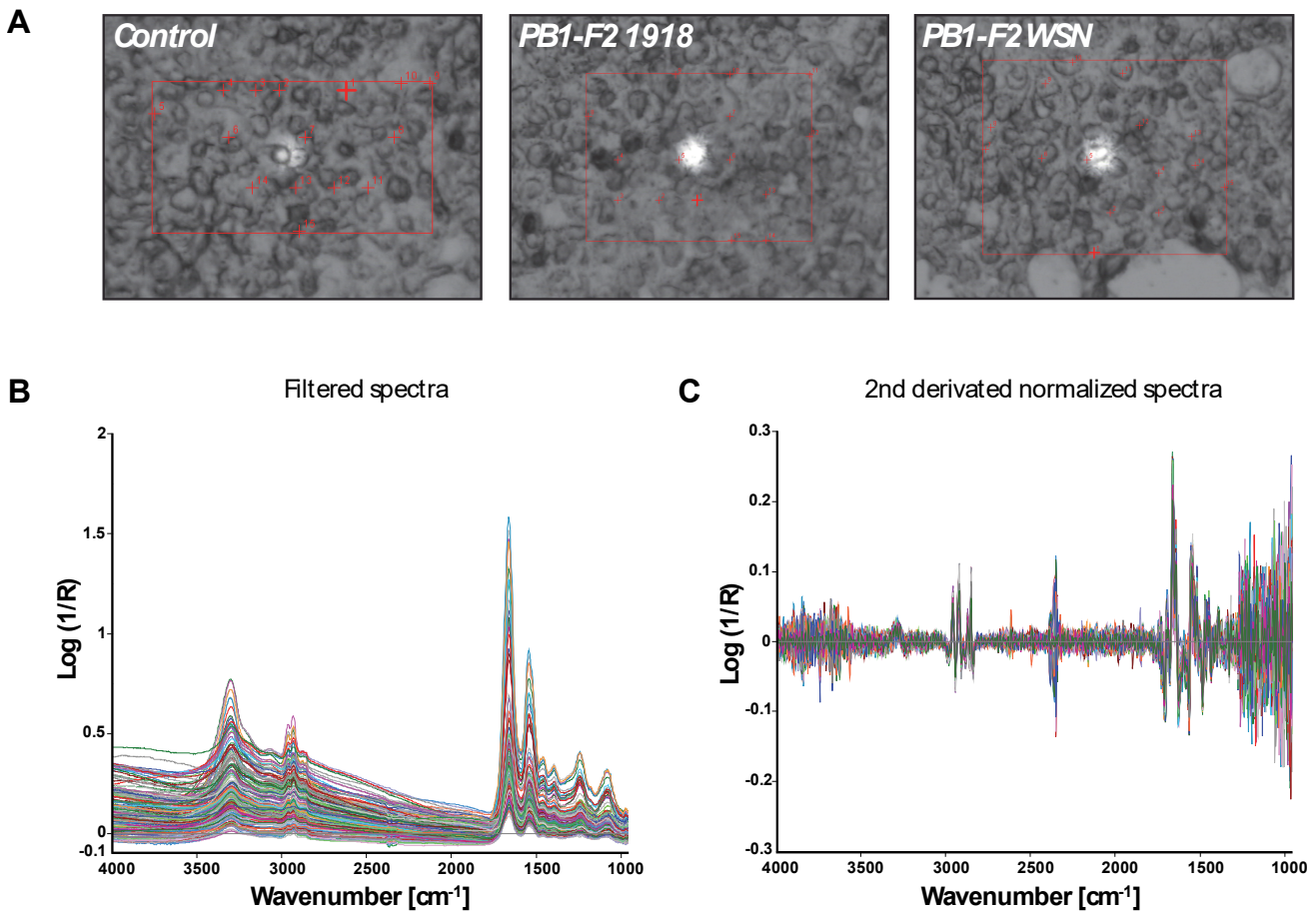

Figure 2. Acquisition and pretreatment of sFT-IR spectromicroscopy data. Human epithelial HEK293T cells were transfected with an empty inducible pTRE-tight vector (control), or an inducible pTRE-tight vector expressing PB1-F2 from A/WSN/1933 (H1N1) (PB1-F2 WSN) or A/Brevig Mission/1/1918 (H1N1) (PB1-F2 1918) viruses. Twenty-four hours post-transfection, the cells were stimulated with 1 µg mL^{-1} doxycycline for 24 h in order to induce expression of PB1-F2. After fixing with paraformaldehyde, the cells were analysed by sFT-IR spectromicroscopy. Seventy-five single-cell IR spectra were recorded for each experimental condition. Representative transmission images of each experimental condition are shown in A. Each red cross corresponds to the acquisition of a single-cell IR spectrum. B: Raw IR spectra retained for the PCA analysis after withdrawal of spectra presenting an irregular baseline. C: Second derivative spectra obtained using the Savitzky–Golay method (nine points segment and third order of polynomial) and the unit vector normalisation in the 4000–950 cm^{-1} range.

region revealed three clusters partially independent using the first (PC1) and second (PC2) components that represent 26% and 5% of the variance, respectively (Figure 3A). Along the PC2 axis, the PB1-F2 WSN cluster was clearly separated from the PB1-F2 1918 and control clusters. The loading plot corresponding to PC2 showed a main peak around 1525 cm^{-1} in the positive direction of this component (Figure 3B). This peak has been previously ascribed to β-sheet structures.[57–59] In the negative direction of PC2, the main variation was due to a peak at 1517 cm^{-1} which has been assigned to tyrosine ring vibrations[60] or α-helix structures.[61] This result might reflect differences in the conformational organisation of PB1-F2 WSN and PB1-F2 1918. We have notably shown in a previous study that the propensity of PB1-F2 to form β-sheet structures varies greatly depending on viral strain.[26] Therefore, the PCA analysis of the amide II region might revealed a higher content of β-sheet structures in PB1-F2 WSN than in PB1-F2 1918.

Altogether, our data suggest that the expression of PB1-F2 WSN and PB1-F2 1918 in HEK293T cells does not induce the formation of aggregated β-sheet structures. This result is in agreement with what we observed in IAV-infected A549 and HeLa cells,[30] pointing

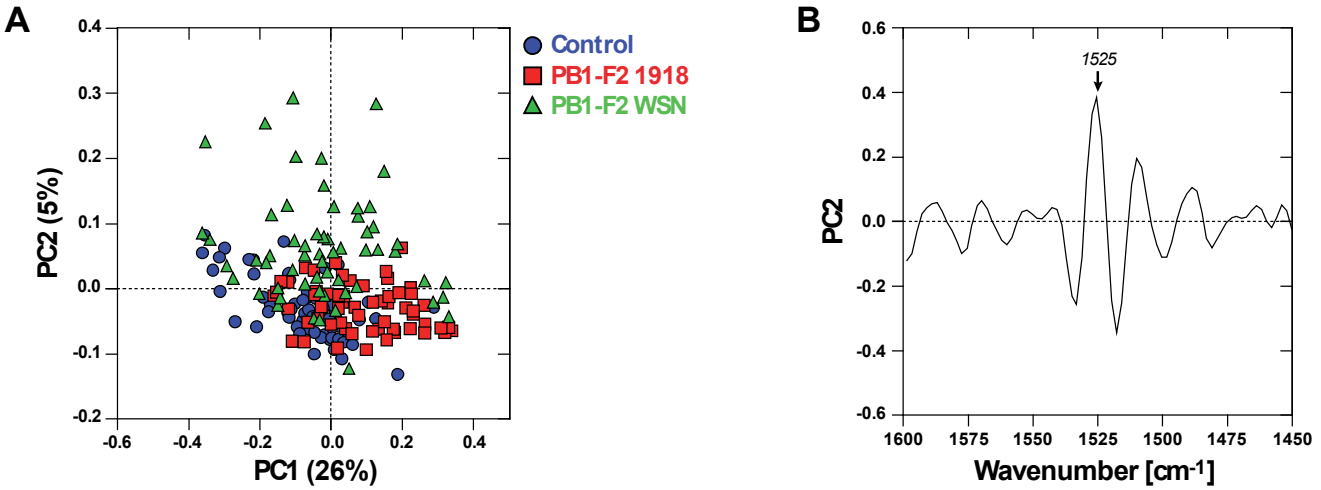

Figure 3. sFT-IR spectromicroscopy analysis of control-, PB1-F2 WSN- and PB1-F2 1918-transfected HEK293T cells in the amide II region. A: PCA score plot of PC1 against PC2 for IR spectra in the 1600–1450 cm^{-1} region of the spectrum. Numbers in brackets correspond to the percentage of the total variance explained by each PC. Each blue circle, red square and green triangle represents a single-cell IR spectrum collected from empty-vector (control)-, PB1-F2 1918- and PB1-F2 WSN-transfected HEK293T cells, respectively. B: Loading plot indicating the influence of the variables (i.e. wavenumber here) that are taken into account in the determination of PC2 by PCA. The wavenumber (1525 cm^{-1}) that most influences the determination of PC2 is indicated by an arrow.

out that the structural conformation of PB1-F2 varies widely between immune (e.g. U937) and epithelial cells. Interestingly, it has previously been shown that PB1-F2 induces apoptosis in immune cells,[48,62–64] but not in epithelial cells.[11,62,65] Moreover, it has been demonstrated that fragmented PB1-F2 amyloid fibres are cytotoxic contrary to mature amyloid fibres.[29] Thus, one may assume that PB1-F2's ability to form amyloid fibres has an effect on its ability to induce apoptosis in a cell-type dependent manner.

PB1-F2 expression does not affect cellular membrane integrity in HEK293T cells

PB1-F2 has been shown to form non-selective channels in phospholipid bilayer membranes, to permeabilise liposomes and damage cell membranes.[26,29,50,66] We have also observed by sFT-IR spectromicroscopy that PB1-F2 expression is associated to a disturbance of membrane fluidity in infected U937.[30] In this context, we decided to examine the ability of PB1-F2 by itself to interfere with membrane integrity in absence of infection in HEK293T cells. We evaluated by sFT-IR analysis the vibrational modes of methyl (CH_3) and methylene (CH_2) groups which mainly result from lipids. Symmetric and asymmetric stretching vibration of CH_3 and CH_2 result in absorption bands in the 3000–2800 cm^{-1} region of the spectrum. However, PCA did not reveal any differences between the control, PB1-F2 WSN and PB1-F2 1918 clusters (Figure S2). Examination of the mean IR spectra indicated that absorption bands assigned to CH_3 (2956 and 2871 cm^{-1}) and CH_2 (2925 and 2854 cm^{-1}) completely overlap the three clusters (Figure 4). This result is very different from what we previously observed in infected U937 and A549 cells.[30] In infected U937 cells, we noticed a distinct shift of the peaks at 2956, 2925, 2871 and 2854 cm^{-1} toward lower wavenumbers only when the virus was able to express PB1-F2. This phenomenon reflected modification of the composition and fluidity of cell membranes, which was attributable to the presence of β-aggregated structures. In A549 cells, we detected a mark difference in CH_2/CH_3 absorbance intensity ratio between non-infected and wild-type WSN virus-infected cells. This result, which is correlated to modulation of apoptosis,[67] was attributed to the cytopathic effect of the virus on epithelial cells, but not to the presence of PB1-F2.

Altogether, our data indicate that transient expression of PB1-F2 in HEK293T cells does not lead to a noticeable destabilisation of cellular membranes, as observed in infected A549 cells. This feature appears to be specific to epithelial cells since a detrimental effect of PB1-F2 on membranes is detected in infected U937 cells. In contrast,

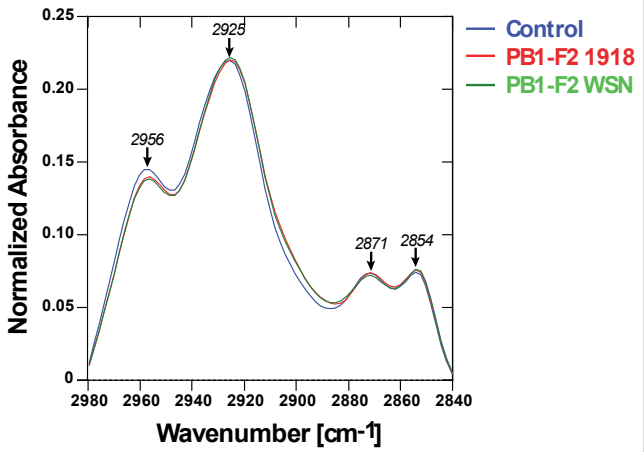

Figure 4. Average spectra in the CH_2/CH_3 (2980–2840 cm^{-1}) region of the spectrum for control-, PB1-F2 WSN- and PB1-F2 1918-transfected HEK293T cells. The average spectra are calculated after performing baseline correction and unit vector normalisation in the 2980–2840 cm^{-1} region. Peaks associated to symmetric and asymmetric CH_2 (2925 and 2854 cm^{-1}, respectively) or CH_3 (2956 and 2871 cm^{-1}, respectively) vibrations are indicated by arrows.

one may assume that the PB1-F2-mediated damage of cellular membranes may contribute to excess cell death in immune cells.

PB1-F2 WSN disrupts mitochondrial functions in HEK293T cells

To gain a comprehensive and unbiased overview of the impact of PB1-F2 on the biochemical composition of HEK293T cells, we explored the 1400–1100 cm^{-1} fingerprint region of the spectrum. The IR spectra of control-, PB1-F2 WSN- and PB1-F2 1918-transfected cells were submitted to PCA and the resulting score plot in this region of the spectrum is presented in Figure 5A. The two first components identified by this analysis, PC1 and PC2, explain 14% and 11% of the total variance. Following the PC1 axis, we notice a clear separation of the PB1-F2 WSN cluster from the control and PB1-F2 1918 clusters. The loading plot associated with PC1 revealed that this separation is mainly based on a difference in the absorbance spectrum at 1238 cm^{-1} (Figure 5B). This band is assigned to an asymmetric PO_2^- stretching vibration which is mainly related to nucleic acids and phospholipids.[68] However, it has also been shown that an absorbance change at this wavenumber can be due to production of ATP.[69,70] In the cell, the majority of ATP is produced in mitochondria through oxidative phosphorylation.[71] Given that PB1-F2 is able to localise within the mitochondria, we propose that the change at 1238 cm^{-1} results from a PB1-F2-induced alteration of mitochondrial activity. Comparison of the mean IR spectra of the three clusters indicates a clear decrease of the absorbance band at 1238 cm^{-1} in PB1-F2 WSN-transfected cells with respect to the other conditions (Figure 5C). Interestingly, PB1-F2 WSN possesses the I68-L69-V70 motif (Figure 1) which has been demonstrated to promote targeting of PB1-F2 to mitochondria.[49] Conversely, this motif is not present in PB1-F2 1918. It has notably been shown that the subcellular localisation of PB1-F2 varies widely among strains.[48,49] Some PB1-F2 variants are almost exclusively present in mitochondria, whereas some others are distributed throughout the cell. This feature can therefore explain the difference observed between PB1-F2 WSN and PB1-F2 1918 regarding the signal intensity at 1238 cm^{-1}. We and others have previously shown that production of ATP by the oxidative phosphorylation mechanism is required for optimal IAV replication.[72,73] Consequently, one may assume that a deleterious effect of PB1-F2 on mitochondrial functions can impact viral fitness. This phenomenon may explain the wide diversity observed among strains regarding the subcellular localisation of PB1-F2 and may play a part in IAV crossing species barrier.

Conclusion

The IAV virulence factor PB1-F2 presents a high polymorphism of sequence and a wide structural diversity. Moreover, the cellular activity of PB1-F2 and its structural conformation appear to be cell-type dependent. While PB1-F2 has been shown to promote apoptosis and to form aggregated β-sheet structures in infected immune cells, neither phenomenon has been correlated with PB1-F2 in infected epithelial cells. This study sought to gain insight on both the structural conformation adopted by PB1-F2 in epithelial cells and the effect of PB1-F2 on the cellular integrity of these cells. To address these questions, we took advantage of sFT-IR spectromicroscopy, which is a very sensitive and a non-destructive technique that offers the possibility to have a snapshot of the overall chemical composition of the cell. sFT-IR spectromicroscopy was performed on human epithelial HEK293T cells that were transfected with expression

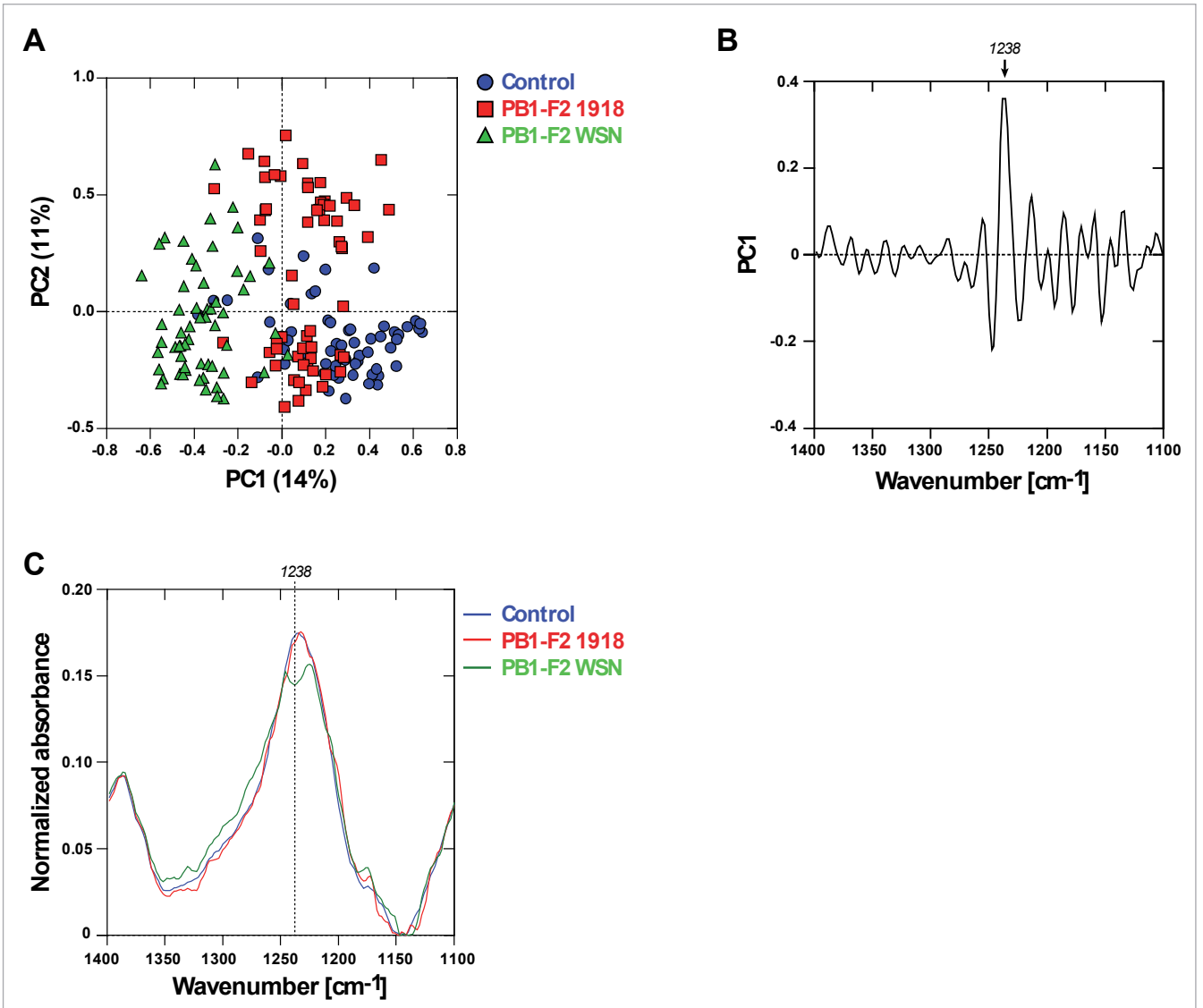

Figure 5. sFT-IR spectromicroscopy analysis of control-, PB1-F2 WSN- and PB1-F2 1918-transfected HEK293T cells in the 1400–1100 cm^{-1} region. A: PCA score plot of PC1 against PC2 for IR spectra in the 1400–1100 cm^{-1} region of the spectrum. Numbers in brackets correspond to the percentage of the total variance explained by each PC. Each blue circle, red square and green triangle represents a single-cell IR spectrum collected from empty-vector (control)-, PB1-F2 1918- and PB1-F2 WSN-transfected HEK293T cells, respectively. B: Loading plot indicating the influence of the variables (i.e. wavenumber here) that are taken into account in the determination of PC1 by PCA. The wavenumber (1238 cm^{-1}) that most influences the determination of PC1 is indicated by an arrow. C: Average spectra in the 1400–1100 cm^{-1} region of the spectrum for each experimental condition. The average spectra are calculated after performing baseline correction and unit vector normalisation in the 1400–1100 cm^{-1} region. The peak assigned to an asymmetric stretching mode of phosphate (PO_2^-) is indicated by a dashed line.

vectors encoding PB1-F2 variants from H1N1 WSN and H1N1 1918 viruses.

Our results suggest that PB1-F2 does not form aggregated β-sheet structures in epithelial cells, corroborating previous findings.[30] In addition, PB1-F2 does not seem to affect membrane integrity in epithelial cells, contrary to what has been observed in immune cells. This difference may explain in part why epithelial cells do not undergo apoptosis in the presence of PB1-F2. Interestingly, even though the amino acid sequences of the two PB1-F2 variants are very similar, sFT-IR analysis revealed a marked difference between PB1-F2 WSN and PB1-F2 1918-transfected cells regarding phosphate vibrations. We assumed that this phenomenon was

related to ATP production in mitochondria because one of the two variants (PB1-F2 WSN) possesses an amino acid motif responsible for mitochondrial targeting. Given that ATP production has been shown to be important for efficient IAV replication, we assume that PB1-F2 could be deleterious for viral production in a strain-dependent manner. In addition, we may also assume that this aspect plays a part in virus adaptation when IAVs cross the species barrier. Altogether, this study shows that sFT-IR spectromicroscopy is a powerful tool for identifying, in a first approach and in an unsupervised manner, cellular mechanisms altered by viral proteins or viruses.

Acknowledgements

We thank Dr Ervin Fodor for the gift of PB1-F2 gene. We acknowledge SOLEIL for provision of synchrotron beamtime (proposals no. 20110735). This work was supported by the REACTIV ANR project (ANR-17-CE35-0007) and the Conseil Régional Ile-de-France through DIM Malinf ("Domaine d'Intérêt Majeur maladies infectieuses, parasitaires et nosocomiales émergentes", grant no. DIM100157).

References

1. R. Gasparini, D. Amicizia, P.L. Lai and D. Panatto, "Clinical and socioeconomic impact of seasonal and pandemic influenza in adults and the elderly", *Hum. Vaccin. Immunother.* **8(1),** 21 (2012). https://doi.org/10.4161/hv.8.1.17622
2. J.S. Long, B. Mistry, S.M. Haslam and W.S. Barclay, "Host and viral determinants of influenza A virus species specificity", *Nat. Rev. Microbiol.* **17(2),** 67 (2019). https://doi.org/10.1038/s41579-018-0115-z
3. F. Krammer, G.J.D. Smith, R.A.M. Fouchier, M. Peiris, K. Kedzierska, P.C. Doherty, P. Palese, M.L. Shaw, J. Treanor, R.G. Webster and A. García-Sastre, "Influenza", *Nat. Rev. Dis. Prim.* **4(1),** 3 (2018). https://doi.org/10.1038/s41572-018-0002-y
4. J.K. Taubenberger and D.M. Morens, "1918 influenza: the mother of all pandemics", *Emerg. Infect. Dis.* **12(1),** 15 (2006). https://doi.org/10.3201/eid1209.05-0979
5. S. Herfst, M. Imai, Y. Kawaoka and R.A.M. Fouchier, *Avian Influenza Virus Transmission to Mammals*. Springer, p. 137 (2014). https://doi.org/10.1007/82_2014_387
6. W.G. Dundon, "Variability among the neuraminidase, non-structural 1 and PB1-F2 proteins in the influenza A virus genome", *Virus Genes* **44(3),** 363 (2012). https://doi.org/10.1007/s11262-012-0714-0
7. J. Buehler, D. Navi, A. Lorusso, A. Vincent, K. Lager and C.L. Miller, "Influenza A virus PB1-F2 protein expression is regulated in a strain-specific manner by sequences located downstream of the PB1-F2 initiation codon", *J. Virol.* **87(19),** 10687 (2013). https://doi.org/10.1128/jvi.01520-13
8. R. Le Goffic, O. Leymarie, C. Chevalier, E. Rebours, B. Da Costa, J. Vidic, D. Descamps, J.-M. Sallenave, M. Rauch, M. Samson and B. Delmas, "Transcriptomic analysis of host immune and cell death responses associated with the influenza A virus PB1-F2 protein", *PLoS Pathog.* **7(8),** e1002202 (2011). https://doi.org/10.1371/journal.ppat.1002202
9. O. Leymarie, G. Jouvion, P.-L. Hervé, C. Chevalier, V. Lorin, J. Lecardonnel, B. Da Costa, B. Delmas, N. Escriou and R. Le Goffic, "Kinetic characterization of PB1-F2-mediated immunopathology during highly pathogenic avian H5N1 influenza virus infection", *PLoS One* **8(3),** e57894 (2013). https://doi.org/10.1371/journal.pone.0057894
10. A. Vidy, P. Maisonnasse, B. Da Costa, B. Delmas, C. Chevalier and R. Le Goffic, "The influenza virus protein PB1-F2 increases viral pathogenesis through neutrophil recruitment and NK cells inhibition", *PLoS One* **11(10),** 1 (2016). https://doi.org/10.1371/journal.pone.0165361
11. R. Le Goffic, E. Bouguyon, C. Chevalier, J. Vidic, B. Da Costa, O. Leymarie, C. Bourdieu, L. Decamps, S. Dhorne-Pollet and B. Delmas, "Influenza A virus protein PB1-F2 exacerbates IFN-β expression of human respiratory epithelial cells", *J. Immunol.* **185(8),** 4812 (2010). https://doi.org/10.4049/jimmunol.0903952
12. J.L. McAuley, M.D. Tate, C.J. MacKenzie-Kludas, A. Pinar, W. Zeng, A. Stutz, E. Latz, L.E. Brown and A. Mansell, "Activation of the NLRP3 inflammasome by IAV virulence protein PB1-F2 contributes to severe pathophysiology and disease", *PLoS Pathog.* **9(5),** e1003392 (2013). https://doi.org/10.1371/journal.ppat.1003392
13. O. Leymarie, L. Meyer, L. Tafforeau, V. Lotteau, B. Da Costa, B. Delmas, C. Chevalier and R. Le Goffic, "Influenza virus protein PB1-F2 interacts with

CALCOCO2 (NDP52) to modulate innate immune response", *J. Gen. Virol.* **98(6),** 1196 (2017). https://doi.org/10.1099/jgv.0.000782

14. A. Pinar, J.K. Dowling, N.J. Bitto, A.A.B. Robertson, E. Latz, C.R. Stewart, G.R. Drummond, M.A. Cooper, J.L. McAuley, M.D. Tate and A. Mansell, "PB1-F2 peptide derived from avian influenza A virus H7N9 induces inflammation via activation of the NLRP3 inflammasome", *J. Biol. Chem.* **292(3),** 826 (2017). https://doi.org/10.1074/jbc.M116.756379

15. O. Leymarie, L. Meyer, P.L. Hervé, B. Da Costa, B. Delmas, C. Chevalier and R. Le Goffic, "Host response comparison of H1N1- and H5N1-infected mice identifies two potential death mechanisms", *Int. J. Mol. Sci.* **18(8),** 1 (2017). https://doi.org/10.3390/ijms18081631

16. J. James, W. Howard, M. Iqbal, V.K. Nair, W.S. Barclay and H. Shelton, "Influenza A virus PB1-F2 protein prolongs viral shedding in chickens lengthening the transmission window", *J. Gen. Virol.* **97(10),** 2516 (2016). https://doi.org/10.1099/jgv.0.000584

17. O. Leymarie, C. Embury-Hyatt, C. Chevalier, L. Jouneau, M. Moroldo, B. Da Costa, Y. Berhane, B. Delmas, H.M. Weingartl and R. Le Goffic, "PB1-F2 attenuates virulence of highly pathogenic avian H5N1 influenza virus in chickens", *PLoS One* **9(6),** (2014). https://doi.org/10.1371/journal.pone.0100679

18. J. James, N. Smith, C. Ross, M. Iqbal, S. Goodbourn, P. Digard, W.S. Barclay and H. Shelton, "The cellular localization of avian influenza virus PB1-F2 protein alters the magnitude of IFN2 promoter and NFκB-dependent promoter antagonism in chicken cells", *J. Gen. Virol.* **100(3),** 414 (2019). https://doi.org/10.1099/jgv.0.001220

19. G.M. Conenello, D. Zamarin, L.A. Perrone, T. Tumpey and P. Palese, "A single mutation in the PB1-F2 of H5N1 (HK/97) and 1918 influenza A viruses contributes to increased virulence", *PLoS Pathog.* **3(10),** 1414 (2007). https://doi.org/10.1371/journal.ppat.0030141

20. G.M. Conenello, J.R. Tisoncik, E. Rosenzweig, Z.T. Varga, P. Palese and M.G. Katze, "A single N66S mutation in the PB1-F2 protein of influenza A virus increases virulence by inhibiting the early interferon response *in vivo*", *J. Virol.* **85(2)**, 652 (2011). https://doi.org/10.1128/JVI.01987-10

21. A.M. Smith and J.A. McCullers, "Molecular signatures of virulence in the PB1-F2 proteins of H5N1 influenza viruses", *Virus Res.* **178(1),** 146 (2013). https://doi.org/10.1016/j.virusres.2013.02.012

22. I. V Alymova, A.M. Green, N. van de Velde, J.L. McAuley, K.L. Boyd, H.E. Ghoneim and J.A. McCullers, "Immunopathogenic and antibacterial effects of H3N2 influenza A virus PB1-F2 map to amino acid residues 62, 75, 79, and 82", *J. Virol.* **85(23),** 12324 (2011). https://doi.org/10.1128/JVI.05872-11

23. P. Gurung, J.R. Lukens and T. Kanneganti, "Mitochondria: diversity in the regulation of the NLRP3 inflammasome", *Trends Mol. Med.* **21(3),** 193 (2015). https://doi.org/10.1016/j.molmed.2014.11.008

24. E. Jo, J.K. Kim, D. Shin and C. Sasakawa, "Molecular mechanisms regulating NLRP3 inflammasome activation", *Cell. Mol. Immunol.* **13(2),** 148 (2015). https://doi.org/10.1038/cmi.2015.95

25. Y. He, H. Hara and G. Núñez, "Mechanism and regulation of NLRP3 inflammasome activation", **41(12),** 1012 (2016). https://doi.org/10.1016/j.tibs.2016.09.002

26. C. Chevalier, A. Al Bazzal, J. Vidic, V. Février, C. Bourdieu, E. Bouguyon, R. Le Goffic, J.-F. Vautherot, J. Bernard, M. Moudjou, S. Noinville, J.-F. Chich, B. Da Costa, H. Rezaei and B. Delmas, "PB1-F2 influenza a virus protein adopts a beta-sheet conformation and forms amyloid fibers in membrane environments", *J. Biol. Chem.* **285(17),** 13233 (2010). https://doi.org/10.1074/jbc.M109.067710

27. A. Miodek, J. Vidic, H. Sauriat-dorizon, C. Richard, R. Le, H. Korri-youssou and C. Chevalier, "Electrochemical detection of the oligomerization of PB1-F2 influenza A virus protein in infected cells", *Anal. Chem.* **86(18),** 9098 (2014). https://doi.org/10.1021/ac5018056

28. A. Miodek, H. Sauriat-Dorizon, C. Chevalier, B. Delmas, J. Vidic and H. Korri-Youssoufi, "Direct electrochemical detection of PB1-F2 protein of influenza A virus in infected cells", *Biosens. Bioelectron.* **59,** 6 (2014). https://doi.org/10.1016/j.bios.2014.02.037

29. J. Vidic, C.A. Richard, C. Péchoux, B. Da Costa, N. Bertho, S. Mazerat, B. Delmas and C. Chevalier, "Amyloid assemblies of influenza A virus PB1-F2 protein damage membrane and induce cytotoxicity",

J. Biol. Chem. **291(2),** 739 (2016). https://doi.org/10.1074/jbc.M115.652917

30. C. Chevalier, R. Le Goffic, F. Jamme, O. Leymarie, M. Réfrégiers and B. Delmas, "Synchrotron infrared and deep UV fluorescent microspectroscopy study of PB1-F2 β-aggregated structures in influenza A virus-infected cells.", *J. Biol. Chem.* **291(17),** 9060 (2016). https://doi.org/10.1074/jbc.M115.710533

31. T. Astruc, F. Peyrin, A. Vénien, R. Labas, M. Abrantes, P. Dumas and F. Jamme, "*In situ* thermal denaturation of myofibre sub-type proteins studied by immunohistofluorescence and synchrotron radiation FT-IR microspectroscopy", *Food Chem.* **134(2),** 1044 (2012). https://doi.org/10.1016/j.foodchem.2012.03.012

32. F. Jamme, J.D. Vindigni, V. Méchin, T. Cherifi, T. Chardot and M. Froissard, "Single cell synchrotron FT-IR microspectroscopy reveals a link between neutral lipid and storage carbohydrate fluxes in *S. cerevisiae*", *PLoS One* **8(9),** 1 (2013). https://doi.org/10.1371/journal.pone.0074421

33. C. Saulou, F. Jamme, C. Maranges, I. Fourquaux, B. Despax, P. Raynaud, P. Dumas and M. Mercier-Bonin, "Synchrotron FTIR microspectroscopy of the yeast *Saccharomyces cerevisiae* after exposure to plasma-deposited nanosilver-containing coating", *Anal. Bioanal. Chem.* **396(4),** 1441 (2010). https://doi.org/10.1007/s00216-009-3316-5

34. L.M. Miller and P. Dumas, "Chemical imaging of biological tissue with synchrotron infrared light", *Biochim. Biophys. Acta Biomembr.* **1758(7),** 846 (2006). https://doi.org/10.1016/j.bbamem.2006.04.010

35. G. Hastings, P. Krug, R. Wang, J. Guo, H.P. Lamichhane, T. Tang, Y.S. Hsu, J. Ward, D. Katz and J. Hilliard, "Viral infection of cells in culture detected using infrared microscopy", *Analyst* **134,** 1462 (2009). https://doi.org/10.1039/b902154j

36. A. Salman, V. Erukhimovitch, M. Talyshinsky, M. Huleihil and M. Huleihel, "FTIR spectroscopic method for detection of cells infected with herpes viruses", *Biopolymers* **67(6),** 406 (2002). https://doi.org/10.1002/bip.10171

37. V. Erukhimovitch, I. Mukmanov, M. Talyshinsky, Y. Souprun and M. Huleihel, "The use of FTIR microscopy for evaluation of herpes viruses infection development kinetics", *Spectrochim. Acta A* **60(10),** 2355 (2004). https://doi.org/10.1016/j.saa.2003.12.009

38. V. Erukhimovitch, M. Talyshinsky, Y. Souprun and M. Huleihel, "FTIR microscopy detection of cells infected with viruses", in *DNA Viruses*, Ed by P.M. Lieberman. Humana Press, pp. 161–172 (2005). https://doi.org/10.1385/1-59259-848-X:161

39. W.D. Duncan and G.P. Williams, "Infrared synchrotron radiation from electron storage rings", *Appl. Opt.* **22(18),** 2914 (1983). https://doi.org/10.1364/AO.22.002914

40. H. Wold, "Path models with latent variables: the NIPALS approach", in *Quantitative Sociology*, Ed by H.M. Blalock. Seminar Press, pp. 307–357 (1975).

41. C.H. Stuart-Harris, "A neurotropic strain of human influenza virus", *Lancet* **233(6027),** 497 (1939). https://doi.org/10.1016/S0140-6736(00)74067-0

42. A.H. Reid, T.G. Fanning, J. V. Hultin and J.K. Taubenberger, "Origin and evolution of the 1918 'Spanish' influenza virus hemagglutinin gene", *Proc. Natl. Acad. Sci.* **96(4),** 1651 (2002). https://doi.org/10.1073/pnas.96.4.1651

43. M. Worobey, G.-Z. Han and A. Rambaut, "Genesis and pathogenesis of the 1918 pandemic H1N1 influenza A virus", *Proc. Natl. Acad. Sci.* **111(22),** 8107 (2014). https://doi.org/10.1073/pnas.1324197111

44. J.L. McAuley, F. Hornung, K.L. Boyd, A.M. Smith, R. McKeon, J. Bennink, J.W. Yewdell and J.A. McCullers, "Expression of the 1918 influenza A virus PB1-F2 enhances the pathogenesis of viral and secondary bacterial pneumonia.", *Cell Host Microbe* **2(4),** 240 (2007). https://doi.org/10.1016/j.chom.2007.09.001

45. A.M. Smith, F.R. Adler, J.L. McAuley, R.N. Gutenkunst, R.M. Ribeiro, J.A. McCullers and A.S. Perelson, "Effect of 1918 PB1-F2 expression on influenza A virus infection kinetics", *PLoS Comput. Biol.* **7(2),** e1001081 (2011). https://doi.org/10.1371/journal.pcbi.1001081

46. H. Yamada, R. Chounan, Y. Higashi, N. Kurihara and H. Kido, "Mitochondrial targeting sequence of the influenza A virus PB1-F2 protein and its function in mitochondria", *FEBS Lett.* **578(3),** 331 (2004). https://doi.org/10.1016/j.febslet.2004.11.017

47. J.S. Gibbs, D. Malide, F. Hornung, J.R. Bennink and J.W. Yewdell, "The influenza A virus PB1-F2 protein targets the inner mitochondrial membrane via a predicted basic amphipathic helix that disrupts

mitochondrial function", **77(13),** 7214 (2003). https://doi.org/10.1128/JVI.77.13.7214

48. C.-J. Chen, G.-W. Chen, C.-H. Wang, C.-H. Huang, Y.-C. Wang and S.-R. Shih, "Differential localization and function of PB1-F2 derived from different strains of influenza A virus", *J. Virol.* **84(19),** 10051 (2010). https://doi.org/10.1128/JVI.00592-10

49. Y.Y. Cheng, S.R. Yang, Y.T. Wang, Y.H. Lin and C.J. Chen, "Amino acid residues 68-71 contribute to influenza A virus PB1-F2 protein stability and functions", *Front. Microbiol.* **8(APR),** 1 (2017). https://doi.org/10.3389/fmicb.2017.00692

50. M. Henkel, D. Mitzner, P. Henklein, F.-J. Meyer-Almes, A. Moroni, M.L. Difrancesco, L.M. Henkes, M. Kreim, S.M. Kast, U. Schubert and G. Thiel, "The proapoptotic influenza A virus protein PB1-F2 forms a nonselective ion channel", *PLoS One* **5(6),** e11112 (2010). https://doi.org/10.1371/journal.pone.0011112

51. I.V. Alymova, A. Samarasinghe, P. Vogel, A.M. Green, R. Weinlich and J.A. McCullers, "A novel cytotoxic sequence contributes to influenza A viral protein PB1-F2 pathogenicity and predisposition to secondary bacterial infection", *J. Virol.* **88(1),** 503 (2014). https://doi.org/10.1128/JVI.01373-13

52. I.V. Alymova, I.A. York and J.A. McCullers, "Non-avian animal reservoirs present a source of influenza A PB1-F2 proteins with novel virulence-enhancing markers", *PLoS One* **9(11),** e111603 (2014). https://doi.org/10.1371/journal.pone.0111603

53. J.L. McAuley, J.E. Chipuk, K.L. Boyd, N. Van De Velde, D.R. Green and J.A. McCullers, "PB1-F2 proteins from H5N1 and 20th century pandemic influenza viruses cause immunopathology.", *PLoS Pathog.* **6(7),** e1001014 (2010). https://doi.org/10.1371/journal.ppat.1001014

54. P. Bassan, H.J. Byrne, F. Bonnier, J. Lee, P. Dumas and P. Gardner, "Resonant Mie scattering in infrared spectroscopy of biological materials–understanding the 'dispersion artefact'", *Analyst* **134(8),** 1586 (2009). https://doi.org/10.1039/b904808a

55. A.M.C. Davies and T. Fearn, "Back to basics : the principles of principal component analysis", *Spectrosc. Eur.* **17(2)**, 20 (2005). https://www.spectroscopyeurope.com/td-column/back-basics-principles-principal-component-analysis

56. L.M. Miller and P. Dumas, "From structure to cellular mechanism with infrared microspectroscopy", *Curr. Opin. Struct. Biol.* **20(5),** 649 (2010). https://doi.org/10.1016/j.sbi.2010.07.007

57. A.L. Jacobson and P.J. Krueger, "Infrared spectroscopic studies of solvent-induced conformational changes in globular proteins", *Biochim. Biophys. Acta Protein Struct.* **393(2),** 274 (1975). https://doi.org/10.1016/0005-2795(75)90054-9

58. M. Jackson and H.H. Mantsch, "The use and misuse of FTIR spectroscopy in the determination of protein structure", *Crit. Rev. Biochem. Mol. Biol.* **30(2),** 95 (1995). https://doi.org/10.3109/10409239509085140

59. A. Adochitel and G. Drochioiu, "Rapid characterization of peptide secondary structure by FT-IR spectroscopy", *Rev. Roum. Chim.* **56(8),** 783 (2011).

60. D.F. Kennedy, A.J. Slotboom, G.H. de Haas and D. Chapman, "A Fourier transform infrared spectroscopic (FTIR) study of porcine and bovine pancreatic phospholipase a2 and their interaction with substrate analogues and a transition-state inhibitor", *Biochim. Biophys. Acta Protein Struct. Mol.* **1040(3),** 317 (1990). https://doi.org/10.1016/0167-4838(90)90129-4

61. K. Kugo, M. Okuno, K. Kitayama, T. Kitaura, J. Nishino, N. Ikuta, E. Nishio and M. Iwatsuki, "Fourier transform IR attenuated total reflectance study on the secondary structure of poly(γ-methyl L-glutamate) surfaces treated with formic acid", *Biopolymers* **32(3),** 197 (1992). https://doi.org/10.1002/bip.360320302

62. W. Chen, P.A. Calvo, D. Malide, J. Gibbs, U. Schubert, I. Bacik, S. Basta, R. O'Neill, J. Schickli, P. Palese, P. Henklein, J.R. Bennink and J.W. Yewdell, "A novel influenza A virus mitochondrial protein that induces cell death", *Nat. Med.* **7(12),** 1306 (2001). https://doi.org/10.1038/nm1201-1306

63. J. Jaworska, F. Coulombe, J. Downey, F. Tzelepis, K. Shalaby, I. Tattoli, J. Berube, S. Rousseau, J.G. Martin, S.E. Girardin, J.A. McCullers and M. Divangahi, "NLRX1 prevents mitochondrial induced apoptosis and enhances macrophage antiviral immunity by interacting with influenza virus PB1-F2 protein", *Proc. Natl. Acad. Sci.* **111(20),** E2110 (2014). https://doi.org/10.1073/pnas.1322118111

64. D. Mitzner, S.E. Dudek, N. Studtrucker, D. Anhlan, I. Mazur, J. Wissing, L. Jänsch, L. Wixler, K. Bruns, A. Sharma, V. Wray, P. Henklein, S. Ludwig and U. Schubert, "Phosphorylation of the influenza A

virus protein PB1-F2 by PKC is crucial for apoptosis promoting functions in monocytes", *Cell. Microbiol.* **11(10),** 1502 (2009). https://doi.org/10.1111/j.1462-5822.2009.01343.x

65. G. Pasricha, S. Mukherjee and A.K. Chakrabarti, "Apoptotic and early innate immune responses to PB1-F2 protein of influenza A viruses belonging to different subtypes in human lung epithelial A549 cells", *Adv. Virol.* **2018,** 5057184 (2018). https://doi.org/10.1155/2018/5057184

66. A.N. Chanturiya, G. Basan, U. Schubert, P. Henklein, J.W. Yewdell and J. Zimmerberg, "PB1-F2, an influenza A virus-encoded proapoptotic mitochondrial protein, creates variably sized pores in planar lipid membranes", **78(12),** 6304 (2004). https://doi.org/10.1128/JVI.78.12.6304

67. F.G. Blankenberg, P.D. Katsikis, R.W. Storrs, C. Beaulieu, D. Spielman, J.Y. Chen, L. Naumovski and J.F. Tait, "Quantitative analysis of apoptotic cell death using proton nuclear magnetic resonance spectroscopy", *Blood* **89(10),** 3778 (1997). https://doi.org/10.1182/blood.V89.10.3778.3778_3778_3786

68. A.C.S. Talari, M.A.G. Martinez, Z. Movasaghi, S. Rehman and I.U. Rehman, "Advances in Fourier transform infrared (FTIR) spectroscopy of biological tissues", *Appl. Spectrosc. Rev.* **52(5),** 456 (2017). https://doi.org/10.1080/05704928.2016.1230863

69. S. Kumar and A. Barth, "Following enzyme activity with infrared spectroscopy", *Sensors* **10(4),** 2626 (2010). https://doi.org/10.3390/s100402626

70. A. Barth, W. Kreutz and W. Mäntele, "Molecular changes in the sarcoplasmic reticulum calcium ATPase during catalytic activity. a Fourier transform infrared (FTIR) study using photolysis of caged ATP to trigger the reaction cycle", *FEBS Lett.* **277(1–2),** 147 (1990). https://doi.org/10.1016/0014-5793(90)80830-C

71. A.M. Van Der Bliek, M.M. Sedensky and P.G. Morgan, "Cell biology of the mitochondrion", *Genetics* **207(3),** 843 (2017). https://doi.org/10.1534/genetics.117.300262

72. L. Meyer, O. Leymarie, C. Chevalier, E. Esnault, M. Moroldo, B. Da Costa, S. Georgeault, P. Roingeard, B. Delmas, P. Quere and R. Le Goffic, "Transcriptomic profiling of a chicken lung epithelial cell line (CLEC213) reveals a mitochondrial respiratory chain activity boost during influenza virus infection", *PLoS One* **12(4),** e0176355 (2017). https://doi.org/10.1371/journal.pone.0176355

73. B. Taye, D. Yeo, R. Lee, B. Tan, R. Sugrue and S. Maurer-Stroh, "Inter-species host gene expression differences in response to human and avian influenza A virus strains", *Int. J. Mol. Sci.* **18(11),** 2295 (2017). https://doi.org/10.3390/ijms18112295